Research Article Vol. 7, No. 3 / March 2019 / Photonics Research 283

PHOTONICS Research

Ternary $ReS_{2(1-x)}Se_{2x}$ alloy saturable absorber for passively Q-switched and mode-locked erbium-doped all-fiber lasers

Chenxi Dou,[1,†] Wen Wen,[2,3,†] Junli Wang,[1,*] Mengyuan Ma,[1] Liming Xie,[2,3] Ching-Hwa Ho,[4] and Zhiyi Wei[5]

[1]School of Physics and Optoelectronics Engineering, Xidian University, Xi'an 710071, China
[2]CAS Key Laboratory of Standardization and Measurement for Nanotechnology, CAS Center for Excellence in Nanoscience, National Center for Nanoscience and Technology, Beijing 100190, China
[3]University of Chinese Academy of Sciences, Beijing 100049, China
[4]Graduate Institute of Applied Science and Technology, National Taiwan University of Science and Technology, Taipei 106, Taiwan
[5]Beijing National Laboratory for Condensed Matter Physics, Institute of Physics, Chinese Academy of Sciences, Beijing 100190, China
*Corresponding author: dispersion@126.com

Received 17 September 2018; revised 17 December 2018; accepted 8 January 2019; posted 9 January 2019 (Doc. ID 346142); published 15 February 2019

We report Q-switched and mode-locked erbium-doped all-fiber lasers using ternary $ReS_{2(1-x)}Se_{2x}$ as saturable absorbers (SAs). The modulation depth and saturable intensity of the film SA are 1.8% and 0.046 MW/cm^2. In Q-switched mechanism output, the pulse was centered at 1531.1 nm with maximum pulse energy and minimum pulse width of 28.29 nJ and 1.07 μs, respectively. In mode-locked operation, the pulse was centered at 1561.15 nm with pulse width of 888 fs, repetition rate of 2.95 MHz, and maximum pulse energy of 0.275 nJ. To the best of our knowledge, this is the first report on the mode-locked Er^{3+}-doped fiber laser using ternary transition metal dichalcogenides. This work suggests prospective 2D-material SAs can be widely used in versatile fields due to their attractive optoelectronic and tunable energy bandgap properties.

https://doi.org/10.1364/PRJ.7.000283

1. INTRODUCTION

In recent years, the discovery of graphene has inspired a wave of 2D-material research, but the zero-band of graphene severely impedes its application in some fields [1,2]. Transition metal dichalcogenides (TMDs), which possess a unique layer-dependent structure and a desirable bandgap by adjusting the layer of the material, are promising in fabricating optical–electronic devices [3–5]. TMDs have a typical atomic structure of MX_2, in which M represents transition metal atoms such as Mo, W, and Re and X represents chalcogen atoms such as S and Se [6]. The transition metal atoms are sandwiched by two layers of chalcogen atoms with a strong chemical bond so that the TMDs can be easily peeled off from a few layers to the monolayer. Moreover, the TMD's bandgap energy depends on its thickness, which decreases while reducing the number of layers, and the TMD even transits from an indirect bandgap to a direct bandgap [7]. Q-switching and mode-locking technologies in fiber lasers have been widely applied to generate ultrafast pulses in remote sensing communication technology, medical surgery, precise optical metrology [8–11], and so on, owing to their compact structure, high beam quality, and stability. Compared to active mode-locking and Q-switching engineering, passive methods with saturable absorbers (SAs) have been more attractive because the system can be constituted in an all-fiber way without a spatial device, greatly improving the stability and simplicity of the oscillator. Therefore, there is a strong requirement in developing new types of SAs. As a member of the SA family, TMDs with unique optical, dynamical, and electronic characteristics have been a promising SA in Q-switching and mode-locking technologies. For instance, the environmentally stable 2D materials MoS_2, WS_2 [12–19], and rhenium dichalcogenides ($ReX_2, X = S, Se$), especially their alloying $ReS_{2(1-x)}Se_{2x}$, have received substantial attention [20–22] due to the fact that their bandgap can be continuously tuned from 1.62 to 1.31 eV by adjusting the S composition from 0 to 1. This unique property is significant for accurate bandgap engineering and, therefore, it is widely used in the fabrication of a functional device with polarization sensitivity [23,24]. Bandgap engineering of a few layers of 2D materials is of great significance in optoelectronics applications. Combining materials with different bandgaps into an alloy could effectively modify their bandgaps not only by changing thickness but also by

changing the parameter x of $ReS_{2(1-x)}Se_{2x}$ [20]. The ternary TMD alloy provides more freedom to regulate its energy bandgap through changing the proportion of two elements, for example, S and Se in the $ReS_{2(1-x)}Se_{2x}$. However, the study of the nonlinear optical properties of ternary 2D $ReS_{2(1-x)}Se_{2x}$ is insufficient, and the application to Q-switched and mode-locked fiber lasers has not been reported yet. In this work, we explore the nonlinear optical properties of the ternary TMD and demonstrate an Er^{3+}-doped all-fiber laser based on ternary 2D $ReS_{2(1-x)}Se_{2x}$ SAs for the first time to our knowledge. We found the Raman spectroscopy and electrical transport of the $ReS_{2(1-x)}Se_{2x}$ ternary alloys with x ranging from 0 to 1. The Raman and electrical signals unambiguously demonstrated the environmental stability of these ternary alloys [25]. By transferring $ReS_{1.02}Se_{0.98}$ fabricated by the chemical vapor deposition method onto the fiber end face and integrating it into the laser cavity, we not only obtained stable mode-locked soliton pulse trains with a pulse duration, repetition rate, and spectrum bandwidth of 880 fs, 2.95 MHz, and 5 nm, respectively, but also realized Q-switched pulse trains with maximum pulse energy of 28.29 nJ and minimum pulse width of 1.070 μs.

2. PREPARATION AND CHARACTERIZATION OF $ReS_{1.02}Se_{0.98}$ SA

$ReS_{2(1-x)}Se_{2x}$ single crystals were grown by the chemical vapor transport method with Br_2 as the transport agent at 1030°C for 10 days [26]. In this case, the $ReS_{1.02}Se_{0.98}$ flakes were prepared by mechanical exfoliation from a single crystal. To validate the successful fabrication of $ReS_{1.02}Se_{0.98}$ 2D flakes, we performed scanning electron microscopy (SEM), atomic force microscopy (AFM), transmission electron microscopy (TEM), and X-ray photoelectron spectroscopy (XPS). The SEM image, together with the energy dispersive spectroscopy (EDS) elemental mapping of S and Se [Fig. 1(a)], illustrates that the S and Se atoms homogeneously distribute on the 2D flake, validating the formation of a $ReS_{1.02}Se_{0.98}$ alloy. The height of the $ReS_{1.02}Se_{0.98}$ flakes was measured on a Veeco Dimension 3100 AFM with tapping mode. SEM imaging was carried out on a Hitachi S-4800 operating at 2.0 kV. The mechanically exfoliated flakes were transferred onto small lacey formvar/carbon film TEM grids (BZ110120A) for TEM imaging and EDS. An FEI Tecnai G2 F20 U-TEIN operated at 200 kV. Raman spectroscopy was done on a micro-Raman spectrometer (Renishaw inVia plus a 514.5 nm laser), with an 1800 lines/mm grating. Photoluminescence was done with a Horiba HR800 Raman system with a liquid-nitrogen-cooled InGaAs detector. XPS was done on an Axis Ultra system. According to the EDS results, the atomic ratio of S:Se is about 0.51:0.49. The AFM image shows a representative 2D flake of 8 nm in height [Figs. 1(b) and 1(c)]. As shown in the high-resolution TEM (HRTEM) image [Fig. 1(d)], a set of lattice planes possess a distance of 3.4 Å (1 Å = 0.1 nm), which can be assigned to the (010) plane. The arrow labeled in Fig. 1(d) illustrates the direction of the Re atomic chain. The composition of the $ReS_{1.02}Se_{0.98}$ flakes is further confirmed by XPS. The XPS spectrum ranging from 157 to 172 eV can be fitted by four peaks of Se $3p^{3/2}$, S $2p^{3/2}$, S $2p^{1/2}$, and Se $2p^{3/2}$, respectively, indicating the alloy of S and Se in the 2D flakes. Owing to the low-symmetry lattice, $ReS_{1.02}Se_{0.98}$ exhibits 18 active Raman modes [Fig. 1(f)]. The

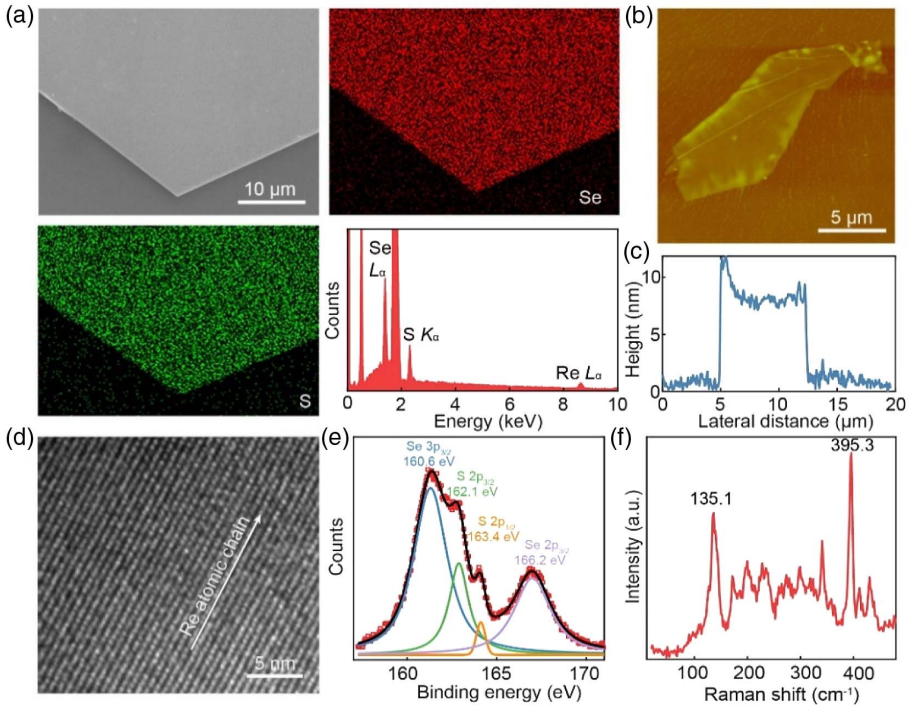

Fig. 1. (a) SEM image, EDS elemental mapping and spectrum of Re, S, and Se. (b) AFM topography, (c) height diagram of a $ReS_{1.02}Se_{0.98}$ flake on a SiO_2/Si substrate. (d) HRTEM image, (e) XPS profiles, and (f) Raman spectra of a $ReS_{1.02}Se_{0.98}$ flake.

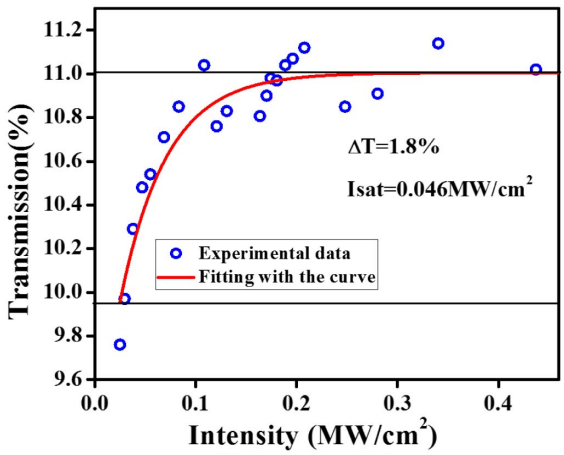

Fig. 2. Nonlinear absorption of a $ReS_{1.02}Se_{0.98}$ SA.

peak at 135.1 cm^{-1} can be attributed to the Ag-like vibration of Re atoms, and the peak at 395.3 cm^{-1} corresponds to the Cp vibration of S and Se atoms [20].

We also measured the nonlinear absorption of the $ReS_{1.02}Se_{0.98}$ film by using the balanced twin-detector method reported in our previous work [27]. A homemade fiber laser with a 1570 nm center wavelength was used as the illuminant. The measured modulation depth was 1.8%, as Fig. 2 shows.

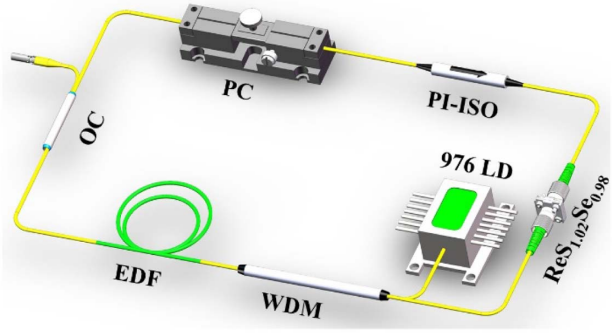

Fig. 3. Schematic of the all-fiber *Q*-switched EDF laser cavity.

3. EXPERIMENT SETUP AND RESULTS

A. *Q*-Switched Erbium-Doped Fiber Laser

The diagram of the experimental setup is illustrated in Fig. 3. The whole setup is a compact structure for good environmental stability. The total length of the laser cavity is 4.76 m corresponding to the dispersion of 0.093 ps^2, which contains 36 cm Er-110-4/125 erbium-doped fiber (EDF). The oscillator also consists of a 980/1550 nm wavelength-division multiplexer, a 20% output optical coupler (OC), a polarization independent isolator (PI-ISO), and a polarization controller (PC). The oscillator is pumped by a diode laser with a wavelength of 976 nm. The pigtail with $ReS_{1.02}Se_{0.98}$ is integrated into the cavity as an SA to facilitate the generation of the short pulse.

The $ReS_{1.02}Se_{0.98}$ SA film is sandwiched into two fiber end faces with a fiber flange in the oscillator, as shown in Fig. 3. When pump power is increased to 190 mW, a *Q*-switching phenomenon emerges. By further improving the pump power to 600 mW, the *Q*-switching pulse trains still exist and remain stable, indicating that it is a high-quality *Q*-switching operation. Figure 4(a) indicates the *Q*-switching pulse trains of the oscilloscope trace and the corresponding minimum single pulse width of 1.070 μs at a pump power of 600 mW. Figure 4(b) shows the radio frequency (RF) spectrum corresponding to the center frequency of 128 kHz with the 100 Hz resolution bandwidth (RBW). We observed only the fundamental and the harmonic frequencies in the RF spectrum [the inset of Fig. 4(b)], further confirming the stability of the *Q*-switching operation. The signal-to-noise ratio (SNR) we measured is 43 dB.

Figure 5(a) shows the evolution of the pulse duration and repetition rate with different input power. With the pump increasing, the repetition rate increases from 75.37 to 152.7 kHz, while the single pulse width decreases from 4.802 to 1.07 μs. Figure 5(b) indicates the tendency of the output power and pulse energy to vary with the increasing input power. They both increase gradually when the pump power rises. The maximum output power and pulse energy are 4.32 mW and 28.29 nJ, respectively. Meanwhile, we also measured the spectrum of the output pulse trains. Figure 5(c) describes the center wavelength of the $ReS_{1.02}Se_{0.98}$-based

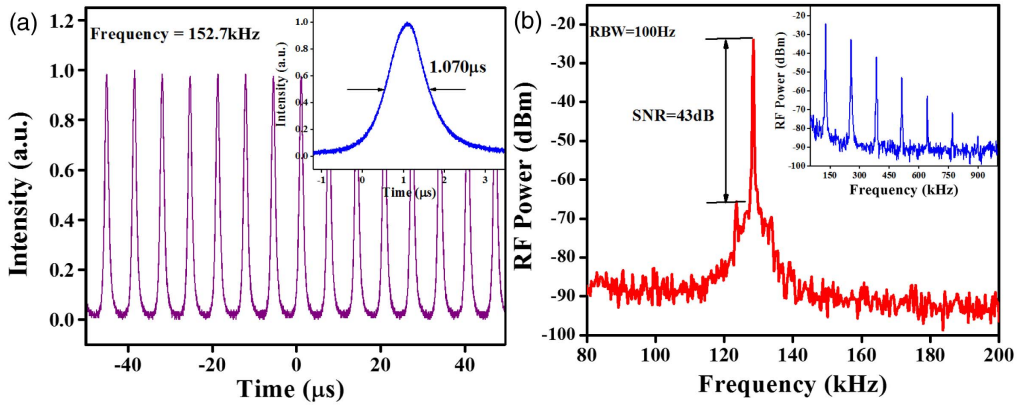

Fig. 4. (a) Pulse trains of *Q*-switching operation at pump power of 600 mW; inset: the corresponding pulse width. (b) RF spectrum (measured with 100 Hz RBW) of *Q*-switching operation with a $ReS_{1.02}Se_{0.98}$ SA at a center frequency of 128 kHz.

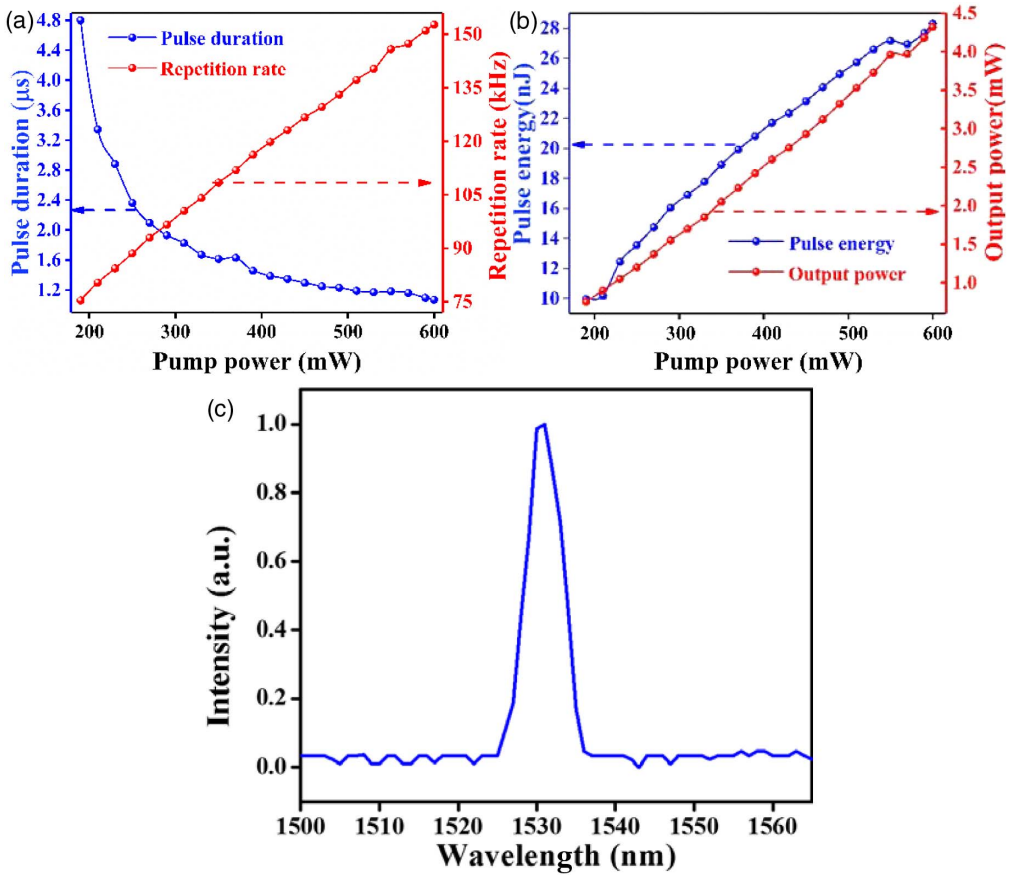

Fig. 5. (a) Pulse duration and repetition rate versus incident pump power of the *Q*-switched mechanism. (b) Output average power and pulse energy versus incident pump power of *Q*-switched operation. (c) The wavelength spectrum of the *Q*-switched EDF laser at the pump power of 300 mW.

Q-switched pulse, which is 1531.1 nm at the pump power of 300 mW.

B. Mode-Locked EDF Laser

The stable *Q*-switching is operated with a total length of 4.76 m, 20% OC, and 36 cm EDF. No matter how we adjust the pump power and polarization state in the cavity, there is no mode-locking phenomenon. To adjust dispersion and eliminate the effect of *Q*-switching instability [28,29], we add a 62.6 m single fiber and use a 78 cm long EDF and 10% OC in the fiber cavity to realize mode-locking operation. Thus, there is a large negative dispersion of −1.46 ps^2 in the cavity, which is helpful to the formation of solitons. In our previous work, we found that the formation of mode-locking operation is related to the polarization state of the laser in the cavity, so we add a PC to regulate it precisely.

In Fig. 6, by adjusting the input power and the PC carefully, the mode-locked pulse trains emerge when the pump power increases to 530 mW. The mode-locked state is quite sensitive to polarization of the laser pulse in the cavity. Figure 7(a) and the inset show the oscilloscope trace of mode-locked pulse trains under a different bandwidth. The interval between adjacent pulses is 338 ns, corresponding to a repetition rate and cavity length of 2.95 MHz and 67.8 m, respectively. Figure 7(b) and the inset indicate the RF spectrum with the

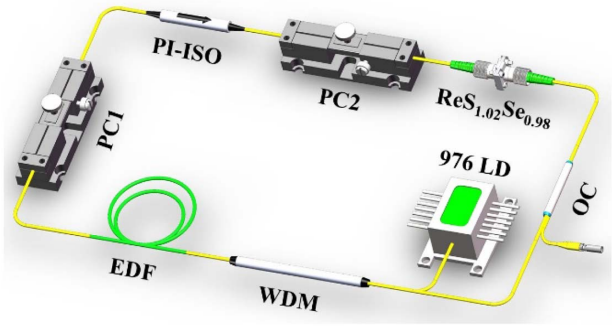

Fig. 6. Diagram of the mode-locked fiber laser setup with a $ReS_{1.02}Se_{0.98}$ SA.

RBW of 100 Hz. The RF output spectrum [the inset of Fig. 7(b)] further confirms the stability of the mode-locking operation. The SNR is 53 dB. We also see from Figs. 7(c) and 7(d), that it possesses a center wavelength of 1561.15 nm and a full width at half-maximum (FWHM) bandwidth of 4.85 nm at 530 mW pump power. There is a characteristic Kelly sideband of a soliton-like spectrum. The optical emission spectrum of the mode-locked Er^{3+}-doped fiber laser was recorded by an optical spectrum analyzer (Horiba IHR550) with

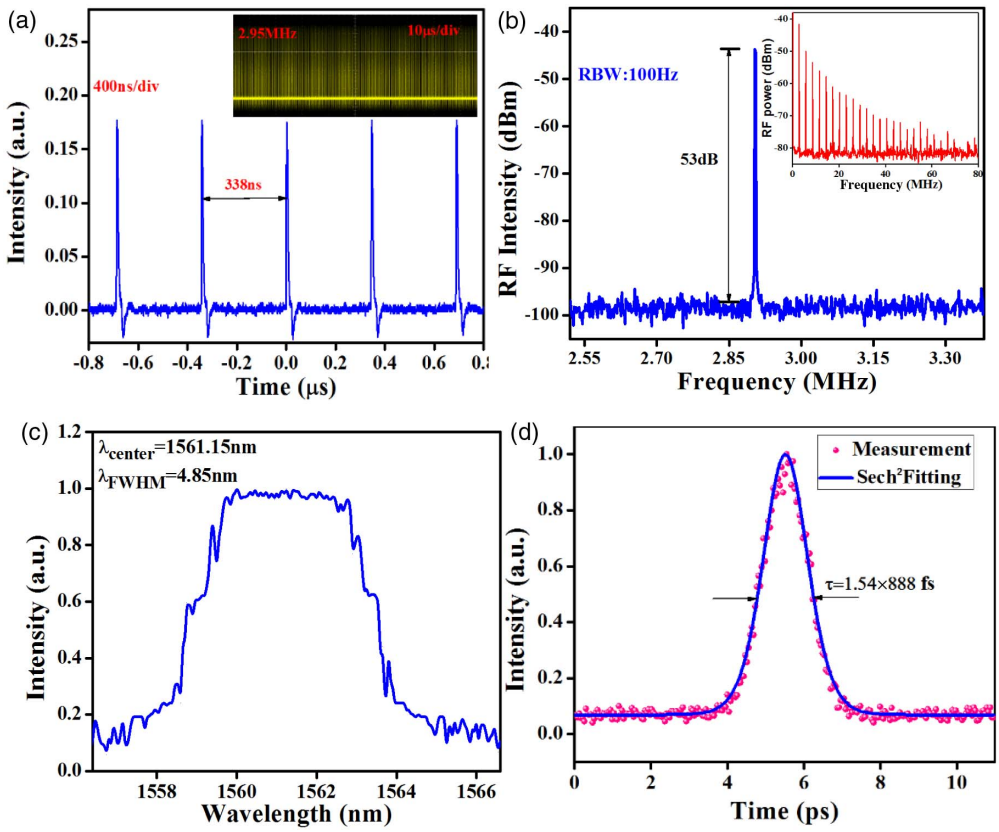

Fig. 7. (a) Pulse trains of mode-locking operation at pump power of 530 mW; inset: oscilloscope trace. (b) RF spectra (measured with 100 Hz RBW) of mode-locking operation with a $ReS_{1.02}Se_{0.98}$ SA at the pump power of 530 mW. (c) Optical spectrum with the bandwidth of 4.85 nm. (d) Autocorrelation trace for output pulse with a pulse duration of 888 fs with $sech^2$ fit.

a resolution of 0.05 nm. In the experiment, the fiber connected with the optical spectrum analyzer to the pulsed laser under test is a multimode fiber, when the measured laser pulses are transmitted from the single-mode fiber to the multimode fiber. This can excite higher-order modes and produce intermode interference; thus, the optical spectrum may not be as clean as expected. By recording the autocorrelation trace of the output trace and fitting the curve with the $sech^2$ function, we measured the pulse duration as 888 fs; this corresponds to a time-bandwidth product (TBP) of 0.53, which indicates that the optical pulse is slightly chirped. The maximum output power is 0.812 mW, corresponding to a single pulse energy of 0.275 nJ, which is much higher than previous reports of rhenium sulfide mode-locked fiber lasers [30–32].

4. SUMMARY

In conclusion, we build the Er^{3+}-doped all fiber laser based on a $ReS_{1.02}Se_{0.98}$ SA to achieve robust *Q*-switched and mode-locked operations. In the *Q*-switched state, we obtain the pulses with a center wavelength of 1531.1 nm and maximum pulse energy and minimum pulse width of 28.29 nJ and 1.07 μs, respectively. In the mode-locked operation, we obtain pulses with a center wavelength of 1561.15 nm with a pulse width of 888 fs. The repetition rate of mode-locking pulse trains is 2.95 MHz, and the maximum pulse energy is up to 0.275 nJ. To the best of our knowledge, this is the first report on a *Q*-switched and mode-locked fiber laser based on a $ReS_{1.02}Se_{0.98}$ SA. We believe that there will be greater potential applications in nonlinear optics and ultrafast photonics. Moreover, the nonlinear optical properties of other $ReS_{2(1-x)}Se_{2x}$ alloys with different atomic proportions also require investigation in the future work.

Funding. National Key R&D Program of China (2018YFB1107200); National Natural Science Foundation of China (NSFC) (61675158, 21673058); Chinese Academy of Sciences Key Project (CAS Key Project) (QYZDB-SSW-SYS031); Chinese Academy of Sciences (CAS) (XDB30000000).

†These authors contributed equally to this work.

REFERENCES

1. J. Liu, S. Wu, Q. H. Yang, and P. Wang, "Stable nanosecond pulse generation from a graphene-based passively Q-switched Yb-doped fiber laser," Opt. Lett. **36**, 4008–4010 (2011).
2. Q. Bao, H. Zhang, Y. Wang, Z. Ni, Y. Yan, and Z. X. Shen, "Atomic-layer graphene as a saturable absorber for ultrafast pulsed lasers," Adv. Funct. Mater. **19**, 3077–3083 (2009).
3. M. Pumera, Z. Sofer, and A. Ambrosi, "Layered transition metal dichalcogenides for electrochemical energy generation and storage," J. Mater. Chem. A **2**, 8981–8987 (2014).

4. J. Wang, Z. Jiang, H. Chen, J. Li, J. Yin, J. Wang, T. C. He, P. G. Yan, and S. C. Ruan, "High energy soliton pulse generation by a magnetron-sputtering-deposition-grown $MoTe_2$ saturable absorber," Photon. Res. **6**, 535–541 (2018).
5. K. Niu, R. Sun, Q. Chen, B. Man, and H. Zhang, "Passively mode-locked Er-doped fiber laser based on SnS_2 nanosheets as a saturable absorber," Photon. Res. **6**, 72–76 (2018).
6. W. S. Yun, S. W. Han, S. C. Hong, I. G. Kim, and J. D. Lee, "Thickness and strain effects on electronic structures of transition metal dichalcogenides: 2H-MX_2 semiconductors (M = Mo, W; X = S, Se, Te)," Phys. Rev. B **85**, 033305 (2012).
7. A. Kuc, N. Zibouche, and T. Heine, "Influence of quantum confinement on the electronic structure of the transition metal sulfide TS_2," Phys. Rev. B **83**, 2237–2249 (2011).
8. M. Skorczakowski, J. Swiderski, W. Pichola, P. Nyga, A. Zajac, M. Maciejewska, L. Galecki, J. Kasprzak, S. Gross, A. Heinrich, and T. Bragagna, "Mid-infrared *Q*-switched Er:YAG laser for medical applications," Laser Phys. Lett. **7**, 498–504 (2010).
9. U. Keller, "Recent developments in compact ultrafast lasers," Nature **424**, 831–838 (2003).
10. M. Merker, R. Ackermann, R. Kammel, K. S. Kunert, and S. Nolte, "An *in vitro* study on focusing fs-laser pulses into ocular media for ophthalmic surgery," Lasers Surg. Med. **45**, 589–596 (2013).
11. F. Morin, F. Druon, M. Hanna, and P. Georges, "Microjoule femtosecond fiber laser at 1.6 μm for corneal surgery applications," Opt. Lett. **34**, 1991–1993 (2009).
12. R. Khazaeizhad, S. H. Kassani, H. Jeong, D. I. Yeom, and K. Oh, "Mode-locking of Er-doped fiber laser using a multilayer MoS_2 thin film as a saturable absorber in both anomalous and normal dispersion regimes," Opt. Express **22**, 23732–23742 (2014).
13. T. H. Chen, C. Y. Lin, Y. H. Lin, Y. C. Chi, C. H. Cheng, Z. Luo, and G. R. Lin, "MoS_2 nano-flake doped polyvinyl alcohol enabling polarized soliton mode-locking of a fiber laser," J. Mater. Chem. C **4**, 1039–1050 (2016).
14. C. Y. Lin, G. R. Lin, T. H. Chen, Z. Luo, and G. R. Lin, "Polarization dependent hybrid mode-locking of erbium-doped fiber laser with MoS_2 saturable absorber," in *Asia Communications and Photonics Conference* (2015), paper AM2B.6.
15. P. Yan, H. Chen, A. Liu, K. Li, S. Ruan, J. Ding, X. Qiu, and T. Guo, "Self-starting mode-locking by fiber-integrated WS_2 saturable absorber mirror," IEEE. J. Sel. Top. Quantum **23**, 1100106 (2016).
16. J. Wang, L. Chen, C. Dou, H. Yan, L. Meng, and Z. Wei, "$Mo_{0.5}W_{0.5}S_2$ for *Q*-switched pulse generation in ytterbium-doped fiber laser," Nanotechnology **29**, 224002 (2018).
17. D. Mao, Y. Wang, C. Ma, L. Han, B. Jiang, X. Gan, S. Hua, W. Zhang, T. Mei, and J. Zhao, "WS_2 mode-locked ultrafast fiber laser," Sci. Rep. **5**, 7965 (2015).
18. X. Li, J. Qian, and F. Ai, "600 fs mode-locked solid-state laser based on few-layer WS_2 saturable absorber," Laser Phys. **28**, 045003 (2018).
19. J. Yin, J. Li, H. Chen, J. Wang, P. Yan, M. Liu, W. Liu, W. Lu, Z. Xu, W. Zhang, J. Wang, Z. Sun, and S. Ruan, "Large-area highly crystalline WSe_2 atomic layers for ultrafast pulsed lasers," Opt. Express **25**, 30020–30031 (2017).
20. W. Wen, J. Lin, K. Suenaga, Y. Guo, Y. Zhu, H.-P. Hsu, and L. Xie, "Preferential S/Se occupation in an anisotropic $ReS_{2(1-x)}Se_{2x}$ monolayer alloy," Nanoscale **9**, 18275–18280 (2017).
21. C. H. Ho, P. C. Liao, Y. S. Huang, T. R. Yang, and K. K. Tiong, "Optical absorption of ReS_2 and $ReSe_2$ single crystals," J. Appl. Phys. **81**, 6380–6383 (1997).
22. R. Zhao, G. Li, B. Zhang, and J. He, "Multi-wavelength bright-dark pulse pair fiber laser based on rhenium disulfide," Opt. Express **26**, 5819–5826 (2018).
23. F. Liu, S. Zheng, X. He, A. Chaturvedi, J. He, W. Chow, T. R. Mion, X. Wang, J. Zhou, Q. Fu, H. Fan, B. K. Tay, L. Song, R. H. He, C. Kloc, P. M. Ajayan, and Z. Liu, "Highly sensitive detection of polarized light using anisotropic 2D ReS_2," Adv. Funct. Mater. **26**, 1146 (2016).
24. S. Tongay, H. Sahin, C. Ko, A. Luce, W. Fan, K. Liu, J. Zhou, Y. S. Huang, C. H. Ho, J. Yan, D. F. Ogletree, S. Aloni, J. Ji, S. Li, J. Li, F. M. Peeters, and J. Wu, "Monolayer behavior in bulk ReS_2 due to electronic and vibrational decoupling," Nat. Commun. **5**, 3252 (2014).
25. W. Wen, Y. Zhu, X. Liu, H. P. Hsu, Z. Fei, Y. Chen, X. Wang, M. Zhang, K. H. Lin, F. S. Huang, Y. P. Wang, Y. S. Huang, Y. P. Wang, Y. S. Huang, C. H. Ho, P. H. Tan, C. Jin, and L. Xie, "Anisotropic spectroscopy and electrical properties of 2D $ReS_{2(1-x)}Se_{2x}$ alloys with distorted 1T structure," Small **13**, 1603788 (2017).
26. C. H. Ho, Y. S. Huang, P. C. Liao, and K. K. Tiong, "Crystal structure and band-edge transitions of $ReS_{2(1-x)}Se_{2x}$ layered compounds," J. Phys. Chem. Sol. **60**, 1797–1804 (1999).
27. J. Wang, C. Dou, L. Chen, H. Yan, L. Meng, J. Zhu, and Z. Wei, "High energy passively *Q*-switched Er^{3+}-doped fiber laser based on $Mo_{0.5}W_{0.5}S_2$ saturable absorber," Opt. Mater. Express **8**, 324–331 (2018).
28. N. Ming, S. Tao, W. Yang, Q. Chen, R. Sun, C. Wang, S. Wang, B. Man, and H. Zhang, "Mode-locked Er-doped fiber laser based on PbS/CdS core/shell quantum dots as saturable absorber," Opt. Express **26**, 9017–9026 (2018).
29. G. Sobon, J. Sotor, K. Grodecki, K. M. Abramski, P. Paletko, and W. Macherzynski, "Mode-locking in Er-doped fiber laser based on mechanically exfoliated Sb_2Te_3 saturable absorber," Opt. Mater. Express **4**, 1–6 (2014).
30. F. Lu, "Passively harmonic mode-locked fiber laser based on ReS_2 saturable absorber," Mod. Phys. Lett. B **31**, 1750206 (2017).
31. D. Mao, X. Cui, X. Gan, M. Li, W. Zhang, H. Lu, and J. Zhao, "Passively *Q*-switched and mode-locked fiber laser based on a ReS_2 saturable absorber," IEEE. J. Sel. Top. Quantum **24**, 1100406 (2017).
32. D. Steinberg, J. D. Zapata, E. A. T. Souza, and L. A. M. Saito, "Mechanically exfoliated rhenium disulfide onto D-shaped optical fiber for sub-300 fs EDFL mode-locking," in *Conference on Lasers and Electro-Optics* (2018), paper SM2N.3.